# Journal Pre-proof

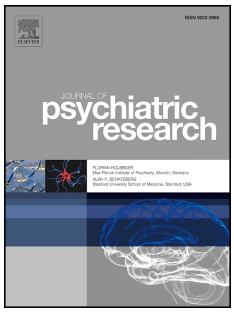

General psychopathology factor (*p*-factor) prediction using resting-state functional connectivity and a scanner-generalization neural network

Jinwoo Hong, Jundong Hwang, Jong-Hwan Lee

PII: S0022-3956(22)00706-3

DOI: https://doi.org/10.1016/j.jpsychires.2022.12.037

Reference: PIAT 5496

To appear in: *Journal of Psychiatric Research*

Received Date: 8 July 2022

Revised Date: 9 December 2022

Accepted Date: 20 December 2022

Please cite this article as: Hong J, Hwang J, Lee J-H, General psychopathology factor (*p*-factor) prediction using resting-state functional connectivity and a scanner-generalization neural network, *Journal of Psychiatric Research* (2023), doi: https://doi.org/10.1016/j.jpsychires.2022.12.037.

# General Psychopathology Factor (*p*-factor) Prediction Using Resting-State Functional Connectivity and a Scanner-Generalization Neural Network

Jinwoo **Hong**, Jundong **Hwang**, Jong-Hwan **Lee**

Department of Brain and Cognitive Engineering, Korea University, Seoul, Republic of Korea



**Short title**: *p*-factor prediction using a deep neural network

***Keywords***: Data harmonization; Deep neural networks; Functional networks; *p*-factor; Psychopathology; Scanner effect

**All correspondence to**:
Jong-Hwan Lee, Ph.D.
Department of Brain and Cognitive Engineering
Korea University
Anam-ro 145, Seongbuk-gu
Seoul 02841
Republic of Korea
E-mail: jonghwan_lee@korea.ac.kr
Tel: +82-2-3290-5922
Fax: +82-2-3290-3667

# Abstract

The general psychopathology factor (*p*-factor) represents shared variance across mental disorders based on psychopathologic symptoms. The Adolescent Brain Cognitive Development (ABCD) Study offers an unprecedented opportunity to investigate functional networks (FNs) from functional magnetic resonance imaging (fMRI) associated with the psychopathology of an adolescent cohort ($n$ > 10,000). However, the heterogeneities associated with the use of multiple sites and multiple scanners in the ABCD Study need to be overcome to improve the prediction of the *p*-factor using fMRI. We proposed a scanner-generalization neural network (SGNN) to predict the individual *p*-factor by systematically reducing the scanner effect for resting-state functional connectivity (RSFC). We included 6,905 adolescents from 18 sites whose fMRI data were collected using either Siemens or GE scanners. The *p*-factor was estimated based on the Child Behavior Checklist (CBCL) scores available in the ABCD study using exploratory factor analysis. We evaluated the Pearson's correlation coefficients (CCs) for *p*-factor prediction via leave-one/two-site-out cross-validation (LOSOCV/LTSOCV) and identified important FNs from the weight features (WFs) of the SGNN. The CCs were higher for the SGNN than for alternative models when using both LOSOCV (0.1631 ± 0.0673 for the SGNN vs. 0.1497 ± 0.0710 for kernel ridge regression [KRR]; $p < 0.05$ from a two-tailed paired *t*-test) and LTSOCV (0.1469 ± 0.0381 for the SGNN vs. 0.1394 ± 0.0359 for KRR; $p = 0.01$). It was found that (a) the default-mode and dorsal attention FNs were important for *p*-factor prediction, and (b) the intra-visual FN was important for scanner generalization. We demonstrated the efficacy of our novel SGNN model for *p*-factor prediction while simultaneously eliminating scanner-related confounding effects for RSFC.

# 1. Introduction

Mental disorders often begin during childhood or adolescence and transition from adolescence to adulthood (Caspi et al., 2020). However, traditional diagnostic nosology is limited in its ability to diagnose and treat mental disorders due to high rates of comorbidity (Caspi et al., 2020), pervasive co-occurrence (Sha et al., 2019), and complex heterogeneity (5). Thus, there has been growing interest in alternative transdiagnostic approaches such as the Research Domain Criteria Initiative (RDoC) (Kozak and Cuthbert, 2016) and the Hierarchical Taxonomy of Psychopathology (HiTOP) (Kotov et al., 2021, 2017). The general psychopathology factor (*p*-factor) in the HiTOP is a single latent dimension underlying the structure of psychopathology (Caspi et al., 2014) that represents shared variance across a wide range of mental disorders (Michelini et al., 2019). The efficacy of the *p*-factor has consistently been demonstrated (Caspi and Moffitt, 2018; Laceulle et al., 2020).

Neural substrates for the *p*-factor have been investigated using functional networks (FNs) obtained from resting-state functional magnetic resonance imaging (rfMRI). The utility of rfMRI in investigating various mental disorders has been demonstrated (Canario et al., 2021; Hull et al., 2017; Mwansisya et al., 2017; Parkes et al., 2021), and this has been facilitated by the emergence of large-scale neuroimaging datasets (Martino et al., 2014; Smith et al., 2013; Thompson et al., 2020). Particularly, resting-state functional connectivity (RSFC) has been instrumental in identifying the functional features of rfMRI because, unlike task-based fMRI, there is no task paradigm associated with rfMRI to estimate neuronal activations. Thus, there have been a number of studies investigating the abnormal RSFC features of rfMRI in mental disorders during the developmental period, including general psychopathology (Elliott et al., 2018; Karcher et al., 2021, 2019; Parkes et al., 2020).

Traditionally, statistical approaches and machine learning models have been employed for the analysis of rfMRI datasets (Barber et al., 2019; Kebets et al., 2019; Romer et al., 2021; Sripada et al., 2021;

Xia et al., 2018). However, a significant issue when utilizing large-scale rfMRI datasets is the heterogeneity of the data acquired from different sites. In particular, the diversity of the MRI scanners used in practice has led to non-biological variance in rfMRI datasets (Fortin et al., 2017; Yu et al., 2018). The neutralization of this scanner effect is urgently needed for data harmonization, but it is difficult to simultaneously predict psychopathology and reduce heterogeneity across a dataset using traditional machine learning and statistical models such as ComBat (Beer et al., 2020).

Recently, several studies have employed deep learning techniques such as domain adaptation to reduce or eliminate scanner-related heterogeneity in neuroimaging datasets (Dinsdale et al., 2021; Guan et al., 2021; Zhao et al., 2020). Many of these studies have relied heavily on T1-weighted MRI and diffusion tensor imaging, with only a few focusing on rfMRI (Yu et al., 2018). Moreover, most studies have utilized convolutional neural network (CNN) architectures that have been developed for 2D images or 3D volumes (Schulz et al., 2020; Vu et al., 2020), making them unsuitable for the direct analysis of RSFC in rfMRI because the spatial structure of 2D RSFC patterns is somewhat arbitrarily determined based on the order of the brain regions, unlike 2D image or 3D volume patterns.

In the present study, we were motivated to develop a deep neural network (DNN) to predict the *p*-factor while explicitly modeling the scanner effect on RSFC in a large-scale rfMRI dataset. The efficacy of our proposed scanner-generalization neural network (SGNN) model was evaluated using the Adolescent Brain Cognitive Development (ABCD) Study dataset, which has collected neuroimaging and psychopathological data from over 10,000 adolescents. We hypothesized that the SGNN could identify any close link between the RSFC and the *p*-factor of adolescents in the ABCD study. We also hypothesized that the *p*-factor prediction performance of our SGNN would be superior to machine learning models due to its inclusion of explicit scanner effect generalization. We also investigated the FNs specifically associated with *p*-factor prediction and scanner effect generalization based on the interpretation of the trained SGNN.

# 2. Materials and methods

### *2.1. Participants*

The ABCD study is a longitudinal study in the United States that has collected neuroimaging, behavior, and genetic data from adolescents ($n$ = 11,875; ages 9–10; 52% males) to investigate their biological and behavioral development (https://abcdstudy.org). The ABCD study includes participants with a suitable age range and attendance at a public or private elementary school. Elementary schools were selected from 21 sites based on race and ethnicity, urbanicity, gender, and socioeconomic status, recruiting over 11,000 children, representing over 20% of the entire US population of 9- to 10-year-olds. More details about the recruitment process are available in a previous paper (Garavan et al., 2018). The exclusion criteria were as follows: not being fluent in English or with a parent not fluent in English or Spanish, significant medical or neurological conditions, contraindications to MRI scanning, a gestational age under 28 weeks or a birthweight over 1200 g, a history of traumatic brain injuries, a current diagnosis of schizophrenia, moderate/severe autism spectrum disorder, intellectual disability, and alcohol/substance use disorder. More details regarding the inclusion/exclusion criteria are available in previous studies (Garavan et al., 2018; Michelini et al., 2019). Most of the sites were approved by the central Institutional Review Board (IRB) at the University of California, San Diego, except for some sites with individual site IRBs (e.g., Washington University in St. Louis). All of the procedures were fully explained to the parents or guardians, and the children agreed before participating in the study, with written informed consent provided (Michelini et al., 2019).

We obtained demographic/behavioral data, brain imaging data including structural/functional MRI data, and genetics data from the ABCD study (Casey et al., 2018) 2.0.1 release via the NIMH Data Archive (NDA; https://data-archive.nimh.nih.gov/abcd). Twenty-one sites participated using 3-T MRI scanners for neuroimaging data acquisition (13 sites with the Prisma from Siemens, five sites with the MR750 from GE, and three sites with the Achieva dStream from Philips). The three sites with Philips scanners were excluded

from the analysis because we wanted to evaluate the ability of the proposed SGNN model to generalize the data from two scanners while including as many adolescents as possible. Of the included sites, those subjects (i) whose rfMRI runs did not pass quality control from the ABCD Data Analysis and Informatics Center or (ii) whose Child Behavior Checklist (CBCL) data were missing, meaning that the *p*-factor could not be determined (Achenbach and Rescorla, 2001), were excluded. As a result, 6,905 children across the 18 sites (Table S1) were included (Fig. 1A), with slightly more males (Fig. 1B).

### *2.2. Resting-State Functional Connectivity (RSFC)*

The participants underwent four five-minute rfMRI scans with blood-oxygen-level-dependent (BOLD) contrast acquired using a gradient-echo echo-planar imaging pulse sequence (repetition time = 800 ms; echo time = 30 ms; 2.4 mm isotropic voxel size; flip angle = 90˚). The participants were instructed to open their eyes and fixate on a crosshair on the screen (Casey et al., 2018). The rfMRI data were preprocessed via the ABCD-HCP pipeline (https://github.com/DCAN-Labs/abcd-hcp-pipeline), which is a modification of the HCP pipeline (Glasser et al., 2013). The pipeline included distortion correction, volume alignment, respiration-induced motion filtering, head-motion censoring based on framewise displacement (FD; > 0.2 mm), and projection onto the cortical surface of FreeSurfer (Marek et al., 2019). Details of the imaging parameters for each scanner type and the preprocessing schemes are available in previous reports (Casey et al., 2018).

The preprocessed BOLD rfMRI volumes were parcellated based on the 333 cortical region-of-interest (ROIs) in the Gordon atlas (Gordon et al., 2016) and 19 subcortical ROIs (https://collection3165.readthedocs.io), and the average BOLD time series was obtained for each ROI. We decided to use 13 FNs based on the Gordon atlas because this parcellation scheme has been widely adopted in a number of studies to investigate the abnormal functional features of mental disorders, including general psychopathology, using the RSFC obtained from the ABCD study (Ellwood-Lowe et al., 2021; Karcher et al., 2021; Marek et al., 2019; Michelini et al., 2019; Sripada et al., 2021). The RSFC matrix was then

calculated using Pearson's correlation coefficients (CCs) for the average BOLD time series of paired ROIs, followed by Fisher's r-to-z transformation. We extracted the lower triangular elements from the symmetric RSFC matrix (excluding the diagonal elements) and vectorized them for input into the predictive models. There were 61,776 RSFC edges across the 352 ROIs ($_{352}C_2$; Fig 1C). Each of the 352 ROIs was assigned to one of the 13 FNs (i.e., auditory, cingulo-opercular, cingulo-parietal, dorsal attention [DAN], default-mode [DMN], frontoparietal, retrosplenial-temporal, salience, subcortical, somatomotor-hand [SMH], somatomotor-mouth, ventral attention, and visual [VIS]) or labeled as unassigned.

### *2.3. General Psychopathology Factor (p-factor)*

The *p*-factor is located at the apex of hierarchical dimensional systems derived from the CBCL scores reported by parents via the merging of the externalizing and internalizing dimensions (Michelini et al., 2019). The CBCL scores represent children's behavioral symptoms within the past six months based on 119 items measured on a 3-point scale (0 – not true; 1 – sometimes true; 2 – very true) (Michelini et al., 2019). As the *p*-factor of an individual increases, they can demonstrate higher overall psychopathology, deficits in brain development and cognitive functioning, dysfunction in social communication, and overall life impairment (Caspi and Moffitt, 2018).

### *2.4. Scanner-Generalization Neural Network (SGNN)*

Figure 1D presents our proposed SGNN inspired by domain-adversarial neural networks (Ganin et al., 2015). The goal of the SGNN is to predict the *p*-factor while reducing the scanner-specific heterogeneity for RSFC. Our proposed SGNN model consists of three components: (i) the feature extractor, (ii) the *p*-factor predictor, and (iii) the scanner discriminator. We adopted adversarial learning to train the SGNN. Specifically, the loss term that maximizes the scanner discrimination performance was negatively added to the loss term used to enhance the prediction of the *p*-factor, thus reducing scanner-specific heterogeneity in the *p*-factor prediction process. Please see the supplementary section, "***Training algorithm for our***

***proposed scanner-generalization neural network (SGNN)***." The scanner discriminator was attached to the feature extractor via a gradient reversal layer with control parameter λ (Fig. 1D).

We employed explicit L1-norm regularization, which is a weight sparsity control scheme, to prevent potential overfitting of the SGNN model, thus enhancing the generalization performance (Jang et al., 2017; Kim et al., 2019, 2016). In this scheme, the sparsity level of the weight of each layer was systematically controlled to find an optimal set of features from the high-dimensional input features by pruning irrelevant features (Kim et al., 2016). The SGNN was trained for 150 epochs using the Nesterov accelerated gradient optimizer with a momentum factor of 0.9, a batch size of 32, and a learning rate of $10^{-5}$. The L2 regularization parameter was 0.05. The proposed SGNN was implemented using PyTorch 1.9.1 (https://pytorch.org/) in Python 3.6. The SGNN code and sample data are publicly available at our GitHub repository (https://github.com/bsplku/SGNN).

### *2.5. Leave-One-Site-Out and Leave-Two-Site-Out Cross-Validation*

We aimed to build an SGNN model that was invariant to the MRI scanner effect when predicting the *p*-factor. Thus, we divided the entire dataset into training, validation, and test data based on site information because each site is equipped with its own MRI scanner. Specifically, we adopted nested leave-one-site-out and leave-two-site-out cross-validation (LOSOCV and LTSOCV, respectively) to evaluate the *p*-factor prediction performance (Fig. 2A), thus preventing potential double-dipping issues (Kriegeskorte et al., 2006). The data from one site and two sites were used as independent test samples in the outer loop of the nested LOSOCV and LTSOCV schemes, respectively. The remaining sites were divided into training and validation folds in the inner loop for hyperparameter optimization (i.e., the weight sparsity level in the feature extractor layer and the λ value). One randomly selected Siemens scanner site and another randomly selected GE scanner site were included in the validation fold.

The candidate weight sparsity levels for the feature extractor were set from the lower to higher sparsity level (i.e., 0.5, 0.8, 0.9, 0.975, 0.98, and 0.99, with 1 being the sparsest case), and the candidate $\lambda$ values were 0, 0.002, 0.005, 0.01, and 0.02. The validation performance was obtained for each of the combinatorial scenarios of the two hyperparameters using the validation data based on the mean absolute error (MAE) between the predicted and target *p*-factor scores (Abrol et al., 2021; Schulz et al., 2020). The validation phase was repeated five times for the two randomly selected validation sites, and an optimal set of hyperparameters was selected from the best average validation performance. The prediction performance of the SGNN with the test data was measured using the CCs between the predicted and target *p*-factor scores and their MAE.

We also evaluated the possibility of improving the performance by pre-training either the *p*-factor predictor or scanner discriminator. In pre-training the *p*-factor predictor branch, only the weights/biases of the feature extractor layer and *p*-factor predictor were updated during the pre-training phase while those of the scanner discriminator were frozen until a pre-defined epoch (i.e., from 10 to 50 epochs at intervals of 10). In pre-training the scanner discriminator branch, only the weights/biases of the feature extractor layer and scanner discriminator were updated while those of the *p*-factor predictor branch were frozen until the pre-defined epoch.

### *2.6. Interpretation of the trained SGNN*

We also interpreted the weight features (WFs) of the trained SGNN (Jang et al., 2017; Kim et al., 2019, 2016). Figure 2B illustrates the WF representations obtained by multiplying the weights across the layers. The WF representations for the *p*-factor predictor and scanner discriminator branches obtained from all of the trained models across the CV schemes were averaged (i.e., $n$ = 18 from LOSOCV; $n$ = 65 from LTSOCV). The average WF represented the pairwise weighting factors between the 352 ROIs. The average WF was also interpreted for the FN levels, in which the weighting factors for the WFs in the ROI levels were averaged for each of the 13 FNs (Fig. S3), followed by pseudo-z-scoring. The WFs obtained for the

FN levels provided information on the importance of the FNs for *p*-factor prediction and scanner generalization. The WFs for the ROI level were visualized at a 99.9$^{th}$ percentile threshold (i.e., the edges above the top 0.1% intensity) using BrainNet Viewer ("BrainNet Viewer: A Network Visualization Tool for Human Brain Connectomics," n.d.) for the brain surface and as a circular graph using NeuroMArVL (http://marvl.infotech.monash.edu.au/). We calculated the reliability of the WF patterns for the *p*-factor predictor and scanner discriminator obtained from LOSOCV and LTSOCV via the intraclass correlation coefficients using the pingouin 0.5.0 library in Python 3.6 (Koo and Li, 2016).

### *2.7. Machine Learning models*

We evaluated several machine learning models (available in the Scikit-Learn package 0.24.1 of Python 3.6) for *p*-factor prediction, including logistic regression (LR), LR with L1/L2 regularization (i.e., lasso/ridge regression), kernel ridge regression (KRR) with a radial basis function (RBF), polynomial, and sigmoid function, partial least square regression (PLS), and support vector machine-based regression (SVR). We conducted hyperparameter optimization as much as possible for each of the alternative machine learning models via a grid search using the same sets of training, validation, and test data that were used for the SGNN in the nested LOSOCV/LTSOCV frameworks. The resulting performance obtained from the SGNN and alternative machine learning models was compared using two-tailed paired-sample *t*-tests.

### *2.8. p-factor prediction with age and sex as covariates*

We also performed the *p*-factor prediction by considering age and sex as covariates in the RSFC and *p*-factor. In detail, we regressed out these nuisance variables in the RSFC and *p*-factor using linear regression as follows (Rakesh et al., 2021):

$$\boldsymbol{y} = \boldsymbol{x}_{age}\beta_{age} + \boldsymbol{x}_{sex}\beta_{sex} + \varepsilon,$$

where $\boldsymbol{y}$ is either the original RSFC edge or original *p*-factor score, $\boldsymbol{x}_{age}$ and $\boldsymbol{x}_{sex}$ are age (months) and sex (1 for male and 0 for female) of participants, respectively. Once the parameter estimates ($\beta_{age}$ and $\beta_{sex}$)

were calculated via a least-squares algorithm, the RSFC edge or *p*-factor score that was adjusted using the age and sex confounders was obtained as follows:

$$\hat{\boldsymbol{y}} = \boldsymbol{y} - \left(\boldsymbol{x}_{age}\beta_{age} + \boldsymbol{x}_{sex}\beta_{sex}\right).$$

Using the age/sex-adjusted RSFC edges and *p*-factor scores, we conducted the *p*-factor prediction by deploying SGNN and KRR in the LOSOCV/LTSOCV frameworks. The resulting performance was compared using two-tailed paired-sample *t*-tests.

# 3. Results

### *3.1. p-factor prediction*

The minimum, maximum, mean, and standard deviation of the *p*-factor across all 6,905 participants were −1.721, 3.333, 0.037, and 0.929, respectively. Figures 3 and S4 present the *p*-factor prediction performance for the LOSOCV and LTSOCV, respectively. Overall, the proposed SGNN exhibited superior performance compared to the alternative machine learning models (F-score = 33.36 and $p < 10^{-10}$ from one-way ANOVA). The performance of the SGNN (CC = 0.1631 ± 0.0673; MAE = 0.7411 ± 0.0433) was significantly higher than that of the best performing KRR (CC = 0.1497 ± 0.0710; MAE = 0.7432 ± 0.0438; $p < 0.05$ from a two-tailed paired-sample *t*-test) for LOSOCV (Fig. 3). A similar trend was observed for LTSOCV, though the performance was slightly lower (CC = 0.1469 ± 0.0381 and MAE = 0.7329 ± 0.0233 for SGNN vs. CC = 0.1394 ± 0.0359 and MAE = 0.7344 ± 0.0230 for KRR; $p < 0.05$) (Fig. S4).

Figure S5 illustrates the *p*-factor prediction performance from the SGNN and KRR models by comparing before and after the removal of age/sex-related confounders in the RSFC edges and *p*-factor scores. Overall, prediction performance was compromised after removing age/sex-related confounders. However, the proposed SGNN showed better prediction performance than KRR, the best-performing machine learning model (Fig. 3 and Fig. S4) commonly across the two CV frameworks: (A) LOSOCV (CC

= 0.1419 ± 0.0655 and MAE = 0.7401 ± 0.0459 for SGNN vs. CC = 0.1238 ± 0.0640 and MAE = 0.7419 ± 0.0419 for KRR; $p < 0.05$ from two-tailed paired-sample *t*-test) and (B) LTSOCV (CC = 0.1295 ± 0.0340 and MAE = 0.7348 ± 0.0283 for SGNN vs. CC = 0.1156 ± 0.0335 and MAE = 0.7359 ± 0.0230 for KRR; $p < 0.001$ from two-tailed paired-sample *t*-test).

### *3.2. Hyperparameter tuning and pre-training*

Figure 4 shows the results for hyperparameter tuning and pre-training in LOSOCV. First, high levels of weight sparsity for the feature extractor (i.e., 0.975, 0.98, and 0.99) improved the validation CC performance compared to lower sparsity levels (i.e., 0.5, 0.8, and 0.9) despite the lower CC for the training data, which was indicative of less overfitting ($p < 10^{-10}$ for both the training and validation data from one-way ANOVA; Fig. 4A,B). A moderate level of λ (i.e., 0.01) was selected most frequently as the optimal value for scanner generalization (Fig. 4C) and led to slightly higher validation CCs with a lower degree of overfitting (Fig. 4D). The moderate λ values (i.e., 0.005 and 0.01) produced approximately chance-level accuracy for scanner discrimination (Fig. 4E). The pre-training of weights in the *p*-factor predictor enhanced *p*-factor prediction performance, whereas the pre-training of weights in the scanner discriminator had the opposite effect (Fig. 4F).

### *3.3. Important FNs for p-factor prediction and scanner generalization*

Figure 5 illustrates the WFs of the *p*-factor predictor from the SGNN trained with LOSOCV. Overall, the WF representations for the intra-FNs exhibited strong negative weights within the DAN and within the DMN and strong positive weights between the DAN and DMN and within the VIS (Fig. 5A). The WF representations at the ROI level also showed strong intra- and inter-FN connectivity (Fig. 5B,C). From the WFs of the scanner discriminator, strong positive weights within the VIS network were evident, and moderate negative weights within the DAN, DMN, and SMH were also observed at the FN level (Fig. 6A) and the ROI level (Fig. 6B, C). The WF representations for the SGNN with LTSOCV demonstrated similar

patterns to those with LOSOCV ($r$ = 0.99 for $p$-factor predictor; $r$ = 0.92 for scanner discriminator; corrected $p < 10^{-10}$ for both cases from bootstrap tests with 10,000 iterations; Figs. S6 and S7). The intraclass correlation coefficients for each of the WF patterns in the $p$-factor predictor and scanner discriminator showed reliability levels greater than 0.75.

# 4. Discussion

### *4.1. Summary*

We developed an artificial neural network-based computational model that can predict the $p$-factor using RSFC by explicitly modeling the heterogeneity of the RSFC acquired with multiple scanners across multiple study sites. Our proposed SGNN model was tested with approximately 7,000 subjects across 18 sites from the ABCD Study. The $p$-factor prediction performance of our SGNN model (CC = 0.1631 with LOSOCV and 0.1469 with LTSOCV) was superior to machine learning models (i.e., KRR; CC = 0.1497 and 0.1394; $p < 0.05$). The weight features for the SGNN revealed the importance of intra- and inter-FN connectivity with the DMN and DAN for the prediction of general psychopathology and the potentially influential intra-VIS network connectivity for the generalization of scanner-specific heterogeneity. To the best of our knowledge, this is the first study to show the efficacy of a deep neural network model for $p$-factor prediction among adolescents using RSFC from the ABCD Study while simultaneously removing scanner-related heterogeneity. We believe that our proposed SGNN model can be extended to other large-scale neuroimaging datasets with multiple sites and scanner types and be used to predict other phenotypic characteristics as part of transdiagnostic dimensional approaches in addition to traditional diagnostic labels for mental disorders.

### *4.2. Neural substrates for the general psychopathology of adolescents*

The DMN, known for its pivotal role in self-referential processing, has been consistently reported to be an essential neural signature for a diverse range of symptoms and mental disorders, including attention deficit

hyperactivity disorder (Uddin et al., 2008), depression (Sheline et al., 2009), bipolar disorder, and schizophrenia (Öngür et al., 2010). Furthermore, DMN dysconnectivity has been associated with general psychopathology, especially neurodevelopmental problems (Karcher et al., 2021; Sripada et al., 2021). In line with these studies, based on WF analysis of the SGNN, we found that changes to within-DMN connectivity were a crucial neural substrate for general psychopathology. The WF of the *p*-factor predictor in our SGNN also suggested that within-DAN dysconnectivity was strongly associated with the general psychopathology of adolescents, which is in agreement with recent studies (Brennan et al., 2018; Guo et al., 2018; Karcher et al., 2021; Lees et al., 2021; Sripada et al., 2021). Because the DAN plays an essential role in top-down cognitive control for external stimuli and internal responses, we can infer that within-DAN RSFC impairment reduces general cognitive functioning and increases the risk of general psychopathology (Corbetta et al., 2008; Huang et al., 2018; Zelazo, 2020).

The RSFC between the DMN and DAN has a negative correlation because they are core task-negative and task-positive FNs, respectively (Fox et al., 2005). This negative correlation has a central role in internalizing and externalizing functions (Keller et al., 2015; Whitfield-Gabrieli and Ford, 2012). Thus, abnormalities in this connection (i.e., a weaker negative correlation) have been associated with mental disorders (Esposito et al., 2018; Huang et al., 2018; Spreng et al., 2016). The strong positive weights for the inter-FNs between the DMN and DAN found in the present study are in line with these previous reports. The positive weights within the VIS network were also notable. The VIS network is not commonly regarded as an essential network for psychopathology. However, previous studies have pointed out that dysfunction in visual networks may reflect the impairment of the low-level integration of external visual information, thereby leading to deficits in the higher-order cognitive processing (Elliott et al., 2018; Shaffer et al., 2018; van de Ven et al., 2017).

### *4.3. Neural substrates for scanner effect generalization*

A previous study reported significant heterogeneity in RSFC from the ABCD dataset associated with MRI scanners (i.e., Siemens vs. GE/Philips), particularly within the VIS network (Marek et al., 2019). This was observed using a relatively small number of ABCD samples that were divided into a discovery set ($n$ = 1,166) and a replication set ($n$ = 1,022) with statistical approaches including ANOVA (cf. $n$ = 6,905 for our study). The harmonization of data from multiple sites and scanners is important when seeking to maximize the prediction power using extensive neuroimaging datasets. However, few studies have addressed this by mainly employing statistical methods (Fortin et al., 2017; Yu et al., 2018). Our proposed SGNN is able to reduce this heterogeneity across multiple sites and scanners, simultaneously predicting target values without the need for stringent prior assumptions about the data distribution. In addition to the positive WFs for the within-VIS network, the negative WFs for the within-SMH and within-DMN FNs were also moderately associated with scanner-related heterogeneity, which requires more detailed future research.

### *4.4. SGNN optimization via the weight sparsity level and scanner generalization*

Stringent weight sparsity levels in the feature extractor layer alleviated the degree of overfitting for the SGNN (Fig. 4A, B) because of the lower number of non-zero weights from L1-norm regularization. A weight sparsity level of 0.975 was selected as the optimal level for most of the outer folds (16 of 18). Neither the highest (0.99) nor the lowest (0.5) sparsity levels were selected as optimal, possibly due to slight underfitting (CC = 0.375 ± 0.023 from the training data vs. 0.144 ± 0.011 from the validation data for a sparsity level of 0.99) and substantial overfitting (CC = 0.956 ± 0.002 from the training data vs. 0.074 ± 0.012 from the validation data at 0.5).

The λ parameter also controlled the degree of overfitting. The best validation performance was obtained from a moderate level of λ (i.e., 0.01; Fig. 4C), and the highest λ value exhibited signs of overfitting (Fig. 4D). Scanner generalization was achieved in our SGNN using this hyperparameter (Fig.

4E). When scanner generalization was not considered or only marginal (i.e., $\lambda = 0$ or 0.002), the scanner classification accuracy was substantially higher than chance (i.e., 50%). As the $\lambda$ value increased (i.e., between 0.005 and 0.01), the scanner classification accuracy fell to the level of chance (i.e., the generalized scanner effect), suggesting that the feature extractor layer may have learned the weights that were not sensitive to the two scanners. Larger $\lambda$ values (i.e., 0.02) led to an inversion of the predicted scanners. Other potential hyperparameters such as the learning rate, batch size, number of hidden layers, and number of hidden nodes were fixed to prevent an exhaustive search of the hyperparameters. Thus, it is possible that the prediction performance can be improved further. An optimal pre-training scheme for the weights in the feature extractor layer and the *p*-factor predictor branch of the SGNN (Fig. 4F) may also improve the prediction accuracy for the *p*-factor, which warrants further investigation.

### *4.5. Strengths, limitations, and future work*

The present study has a number of significant implications. First, we developed a novel deep neural network model for *p*-factor prediction by employing domain adaption to reduce the heterogeneity arising from the use of multiple scanners within the large-scale, multiple-site ABCD Study dataset. Our proposed SGNN model exhibited a prediction performance that was superior to alternative machine learning models. We employed thorough cross-validation schemes (i.e., LOSOCV/LTSOCV) to evaluate the performance, unlike previous approaches that did not explicitly consider multiple sites and scanners in CV schemes (Karcher et al., 2021; Wang et al., 2021). Our work and prior studies consistently identified deficits in the RSFC within the DMN and within the DAN as strong evidence associated with general psychopathology. In addition, we reported the relatively novel finding that the *p*-factor increases when the RSFC between the DMN and DAN is a weaker negative correlation based on the strong positive weights for the SGNN between the two FNs. It is worth noting that the essential FNs associated with general psychopathology in the present study were identified using the SGNN model, which minimized multi-scanner heterogeneity within the ABCD Study dataset.

It is also important to note several limitations of the present study and suggest future work. First, we only considered the generalization of two scanners using our SGNN model. We excluded the data acquired from the Philips scanner due to the lack of sites ($n$ = 3) and the relatively low number of subjects ($n$ = 730). Because we employed LOSOCV or LTSOCV to optimize and evaluate our SGNN, there would be only one site with a Philips scanner for the training and validation sets. Our proposed SGNN model can be further validated using other large-scale datasets such as the Philadelphia Neurodevelopmental Cohort (Satterthwaite et al., 2016) and the Human Connectome Project in Development (HCP-D) (Somerville et al., 2018). This future validation could interrogate our reported findings, including the efficacy of our SGNN and the reliability of the extracted FNs for *p*-factor prediction and scanner-effect generalization. Additionally, we only utilized cross-sectional samples from the ABCD Study. Longitudinal samples from this dataset and other cohorts such as the HCP-D would enable the investigation of neural substrates of psychopathology according to the neurodevelopmental phase. Moreover, sex and age also have an impact on both psychopathology and RSFC (Alarcón et al., 2015; Michelini et al., 2019). Our results indicated that the age/sex confounders were helpful for the prediction of the *p*-factor using RSFC (Fig. S5). However, the neuronal signatures of *p*-factor in RSFC have still been preserved after removing these confounders and the *p*-factor prediction performance of SGNN was superior to KRR. We believe that our approach to reducing age/sex-related confounding effects may not be optimal although it has been used in previous study (Rakesh et al., 2021). Alternative approaches such as embedding the age and sex information explicitly into the neural network models can be gainfully utilized (Zhao et al., 2022).

Our work investigated the performance of the SGNN for *p*-factor prediction. Future studies can extend our SGNN model to predict factor scores for low-ranked dimensions such as externalizing and internalizing spectra (Karcher et al., 2021; Michelini et al., 2019). As an extension, neural correlates of the RSFC could be identified in a symptom-specific manner, and neural biomarkers could be validated across psychopathology dimensions in a transdiagnostic system by combining multiple large-scale neuroimaging

datasets. In addition, future work can consider additional validation of the current study by investigating (i) alternative inputs for the SGNN such as dynamic RSFC patterns with sliding windows (Hutchison et al., 2013), (ii) alternative *p*-factor scores from other assessment systems available in the ABCD Study such as the self-reported CBCL and the Kiddie Schedule for Affective Disorders and Schizophrenia (Lees et al., 2021) or the use of alternative techniques to derive the *p*-factor (Barber et al., 2019; Kaczkurkin et al., 2018; Kebets et al., 2019; Norbom et al., 2019; Romer et al., 2021), or (iii) alternative parcellation schemes (Glasser et al., 2013; Shen et al., 2013; Tzourio-Mazoyer et al., 2002).

### *4.6. Conclusions*

We proposed a deep neural network model (SGNN) that can predict the *p*-factor using RSFC and extract associated FNs while simultaneously generalizing the heterogeneity that arises from the use of multiple MRI scanners. We demonstrated the efficacy of our model compared to alternative machine learning models based on its consistently superior *p*-factor prediction performance using systematic cross-validation schemes. We identified novel and reproducible FN features for general psychopathology and scanner generalization. Our proposed method can be employed with cohorts other than adolescents and with alternative large-scale neuroimaging datasets.

# Acknowledgments

This work was supported by a National Research Foundation (NRF) grant from the Ministry of Science and ICT (MSIT) of Korea (NRF-2017R1E1A1A01077288; 2021M3E5D2A01022515). The sponsors were not involved in the study design, data collection, analysis or interpretation of the data, manuscript preparation, or the decision to submit for publication. Authors especially thank Dr. Giorgia Michelini since she kindly provided her research data (i.e., dimensional scores of psychopathologies including *p*-factor of the ABCD participants). The authors also thank Dr. Hyun-Chul Kim, Sungman Jo, and Sangsoo Jin for their help in developing the SGNN model and in conducting statistical tests, and Juhyeon Lee, Minyoung Jeong, and Niv Lustig for their input in evaluating and enhancing the SGNN model, the psychopathology, the visualization of the connectivity patterns, and the preparation of the manuscript. We also thank Soohyun Jeon, Minseok Choi, and JaeEon Kang for their logistical support.

# Conflict of Interest

The authors have no conflicts of interest regarding this study, including financial, consultant, institutional, or other relationships.

# References


Abrol, A., Fu, Z., Salman, M., Silva, R., Du, Y., Plis, S., Calhoun, V., 2021. Deep learning encodes robust discriminative neuroimaging representations to outperform standard machine learning. Nat. Commun. 12. https://doi.org/10.1038/s41467-020-20655-6

Achenbach, T.M., Rescorla, L.A., 2001. Manual for the ASEBA school-age forms & profiles: child behavior checklist for ages 6-18, teacher's report form, youth self-report: an integrated system of multi-informant assessment. University of Vermont, research center for children youth & families.

Alarcón, G., Cservenka, A., Rudolph, M.D., Fair, D.A., Nagel, B.J., 2015. Developmental sex differences in resting state functional connectivity of amygdala sub-regions. NeuroImage 115, 235–244. https://doi.org/10.1016/j.neuroimage.2015.04.013

Barber, A.D., Sarpal, D.K., John, M., Fales, C.L., Mostofsky, S.H., Malhotra, A.K., Karlsgodt, K.H., Lencz, T., 2019. Age-Normative Pathways of Striatal Connectivity Related to Clinical Symptoms in the General Population. Biol. Psychiatry 85, 966–976. https://doi.org/10.1016/j.biopsych.2019.01.024

Beer, J.C., Tustison, N.J., Cook, P.A., Davatzikos, C., Sheline, Y.I., Shinohara, R.T., Linn, K.A., 2020. Longitudinal ComBat: A method for harmonizing longitudinal multi-scanner imaging data. NeuroImage 220. https://doi.org/10.1016/j.neuroimage.2020.117129

BrainNet Viewer: A Network Visualization Tool for Human Brain Connectomics [WWW Document], n.d. URL https://journals.plos.org/plosone/article?id=10.1371/journal.pone.0068910 (accessed 1.3.22).

Brennan, T., Saha, S., Bultan, T., Păsăreanu, C.S., 2018. Symbolic path cost analysis for side-channel detection, in: Proceedings of the 27th ACM SIGSOFT International Symposium on Software Testing and Analysis, ISSTA 2018. Association for Computing Machinery, New York, NY, USA, pp. 27–37. https://doi.org/10.1145/3213846.3213867

Canario, E., Chen, D., Biswal, B., 2021. A review of resting-state fMRI and its use to examine psychiatric disorders. Psychoradiology 1, 42–53. https://doi.org/10.1093/psyrad/kkab003

Casey, B.J., Cannonier, T., Conley, M.I., Cohen, A.O., Barch, D.M., Heitzeg, M.M., Soules, M.E., Teslovich, T., Dellarco, D.V., Garavan, H., Orr, C.A., Wager, T.D., Banich, M.T., Speer, N.K., Sutherland, M.T., Riedel, M.C., Dick, A.S., Bjork, J.M., Thomas, K.M., Chaarani, B., Mejia, M.H., Hagler, D.J., Daniela Cornejo, M., Sicat, C.S., Harms, M.P., Dosenbach, N.U.F., Rosenberg, M., Earl, E., Bartsch, H., Watts, R., Polimeni, J.R., Kuperman, J.M., Fair, D.A., Dale, A.M., 2018. The Adolescent Brain Cognitive Development (ABCD) study: Imaging acquisition across 21 sites. Dev. Cogn. Neurosci. 32, 43–54. https://doi.org/10.1016/j.dcn.2018.03.001

Caspi, A., Houts, R.M., Ambler, A., Danese, A., Elliott, M.L., Hariri, A., Harrington, H.L., Hogan, S., Poulton, R., Ramrakha, S., Rasmussen, L.J.H., Reuben, A., Richmond-Rakerd, L., Sugden, K., Wertz, J., Williams, B.S., Moffitt, T.E., 2020. Longitudinal Assessment of Mental Health Disorders and Comorbidities Across 4 Decades Among Participants in the Dunedin Birth Cohort Study. JAMA Netw. Open 3, e203221. https://doi.org/10.1001/jamanetworkopen.2020.3221

Caspi, A., Houts, R.M., Belsky, D.W., Goldman-Mellor, S.J., Harrington, H., Israel, S., Meier, M.H., Ramrakha, S., Shalev, I., Poulton, R., Moffitt, T.E., 2014. The p factor: One general psychopathology factor in the structure of psychiatric disorders? Clin. Psychol. Sci. 2, 119–137. https://doi.org/10.1177/2167702613497473

Caspi, A., Moffitt, T.E., 2018. All for One and One for All: Mental Disorders in One Dimension. Am. J. Psychiatry 175, 831–844. https://doi.org/10.1176/appi.ajp.2018.17121383

Corbetta, M., Patel, G., Shulman, G.L., 2008. The Reorienting System of the Human Brain: From Environment to Theory of Mind. Neuron 58, 306–324. https://doi.org/10.1016/j.neuron.2008.04.017

Dinsdale, N.K., Jenkinson, M., Namburete, A.I.L., 2021. Deep learning-based unlearning of dataset bias for MRI harmonisation and confound removal. NeuroImage 228, 117689. https://doi.org/10.1016/j.neuroimage.2020.117689

Elliott, M.L., Romer, A., Knodt, A.R., Hariri, A.R., 2018. A Connectome-wide Functional Signature of Transdiagnostic Risk for Mental Illness. Biol. Psychiatry 84, 452–459. https://doi.org/10.1016/j.biopsych.2018.03.012

Ellwood-Lowe, M.E., Whitfield-Gabrieli, S., Bunge, S.A., 2021. Brain network coupling associated with cognitive performance varies as a function of a child's environment in the ABCD study. Nat. Commun. 12, 7183. https://doi.org/10.1038/s41467-021-27336-y

Esposito, R., Cieri, F., Chiacchiaretta, P., Cera, N., Lauriola, M., Di Giannantonio, M., Tartaro, A., Ferretti, A., 2018. Modifications in resting state functional anticorrelation between default mode network and dorsal attention network: comparison among young adults, healthy elders and mild cognitive impairment patients. Brain Imaging Behav. 12, 127–141. https://doi.org/10.1007/s11682-017-9686-y

Fortin, J.-P., Parker, D., Tunç, B., Watanabe, T., Elliott, M.A., Ruparel, K., Roalf, D.R., Satterthwaite, T.D., Gur, R.C., Gur, R.E., Schultz, R.T., Verma, R., Shinohara, R.T., 2017. Harmonization of multi-site diffusion tensor imaging data. NeuroImage 161, 149–170. https://doi.org/10.1016/j.neuroimage.2017.08.047

Fox, M.D., Snyder, A.Z., Vincent, J.L., Corbetta, M., Van Essen, D.C., Raichle, M.E., 2005. The human brain is intrinsically organized into dynamic, anticorrelated functional networks. Proc. Natl. Acad. Sci. U. S. A. 102, 9673–9678. https://doi.org/10.1073/pnas.0504136102

Ganin, Y., Ustinova, E., Ajakan, H., Germain, P., Larochelle, H., Laviolette, F., Marchand, M., Lempitsky, V., 2015. Domain-Adversarial Training of Neural Networks.

Garavan, H., Bartsch, H., Conway, K., Decastro, A., Goldstein, R.Z., Heeringa, S., Jernigan, T., Potter, A., Thompson, W., Zahs, D., 2018. Recruiting the ABCD sample: Design considerations and procedures. Dev. Cogn. Neurosci., The Adolescent Brain Cognitive Development (ABCD) Consortium: Rationale, Aims, and Assessment Strategy 32, 16–22. https://doi.org/10.1016/j.dcn.2018.04.004

Glasser, M.F., Sotiropoulos, S.N., Wilson, J.A., Coalson, T.S., Fischl, B., Andersson, J.L., Xu, J., Jbabdi, S., Webster, M., Polimeni, J.R., Essen, D.C.V., Jenkinson, M., 2013. The minimal preprocessing pipelines for the Human Connectome Project. NeuroImage 80, 105–124. https://doi.org/10.1016/j.neuroimage.2013.04.127

Gordon, E.M., Laumann, T.O., Adeyemo, B., Huckins, J.F., Kelley, W.M., Petersen, S.E., 2016. Generation and Evaluation of a Cortical Area Parcellation from Resting-State Correlations. Cereb. Cortex 26, 288–303. https://doi.org/10.1093/cercor/bhu239

Guan, H., Liu, Y., Yang, E., Yap, P.T., Shen, D., Liu, M., 2021. Multi-site MRI harmonization via attention-guided deep domain adaptation for brain disorder identification. Med. Image Anal. 71. https://doi.org/10.1016/j.media.2021.102076

Guo, W., Zhang, F., Liu, F., Chen, J., Wu, R., Chen, D.Q., Zhang, Z., Zhai, J., Zhao, J., 2018. Cerebellar abnormalities in first-episode, drug-naive schizophrenia at rest. Psychiatry Res. Neuroimaging 276, 73–79. https://doi.org/10.1016/j.pscychresns.2018.03.010

Huang, M., Zhou, F., Wu, L., Wang, B., Wan, H., Li, F., Zeng, X., Gong, H., 2018. Synchronization within, and interactions between, the default mode and dorsal attention networks in relapsing-remitting multiple sclerosis. Neuropsychiatr. Dis. Treat. 14, 1241–1252. https://doi.org/10.2147/NDT.S155478

Hull, J.V., Dokovna, L.B., Jacokes, Z.J., Torgerson, C.M., Irimia, A., Van Horn, J.D., 2017. Resting-State Functional Connectivity in Autism Spectrum Disorders: A Review. Front. Psychiatry 7, 205. https://doi.org/10.3389/fpsyt.2016.00205

Hutchison, R.M., Womelsdorf, T., Allen, E.A., Bandettini, P.A., Calhoun, V.D., Corbetta, M., Della Penna, S., Duyn, J.H., Glover, G.H., Gonzalez-Castillo, J., Handwerker, D.A., Keilholz, S., Kiviniemi, V., Leopold, D.A., de Pasquale, F., Sporns, O., Walter, M., Chang, C., 2013. Dynamic functional connectivity: Promise, issues, and interpretations. NeuroImage, Mapping the Connectome 80, 360–378. https://doi.org/10.1016/j.neuroimage.2013.05.079

Jang, H., Plis, S.M., Calhoun, V.D., Lee, J.-H., 2017. Task-specific feature extraction and classification of fMRI volumes using a deep neural network initialized with a deep belief network: Evaluation using sensorimotor tasks. NeuroImage, Individual Subject Prediction 145, 314–328. https://doi.org/10.1016/j.neuroimage.2016.04.003

Kaczkurkin, A.N., Moore, T.M., Calkins, M.E., Ciric, R., Detre, J.A., Elliott, M.A., Foa, E.B., Garcia de la Garza, A., Roalf, D.R., Rosen, A., Ruparel, K., Shinohara, R.T., Xia, C.H., Wolf, D.H., Gur, R.E., Gur, R.C., Satterthwaite, T.D., 2018. Common and dissociable regional cerebral blood flow differences associate with dimensions of psychopathology across categorical diagnoses. Mol. Psychiatry 23, 1981–1989. https://doi.org/10.1038/mp.2017.174

Karcher, N.R., Michelini, G., Kotov, R., Barch, D.M., 2021. Associations Between Resting-State Functional Connectivity and a Hierarchical Dimensional Structure of Psychopathology in Middle Childhood. Biol. Psychiatry Cogn. Neurosci. Neuroimaging 6, 508–517. https://doi.org/10.1016/j.bpsc.2020.09.008

Karcher, N.R., O'Brien, K.J., Kandala, S., Barch, D.M., 2019. Resting-state functional connectivity and psychotic-like experiences in childhood: results from the adolescent brain cognitive development study. Biol. Psychiatry 86, 7–15.

Kebets, V., Holmes, A.J., Orban, C., Tang, S., Li, J., Sun, N., Kong, R., Poldrack, R.A., Yeo, B.T.T., 2019. Somatosensory-Motor Dysconnectivity Spans Multiple Transdiagnostic Dimensions of Psychopathology. Biol. Psychiatry 86, 779–791. https://doi.org/10.1016/j.biopsych.2019.06.013

Keller, J.B., Hedden, T., Thompson, T.W., Anteraper, S.A., Gabrieli, J.D.E., Whitfield-Gabrieli, S., 2015. Resting-state anticorrelations between medial and lateral prefrontal cortex: Association with working memory, aging, and individual differences. Cortex 64, 271–280. https://doi.org/10.1016/j.cortex.2014.12.001

Kim, H.C., Bandettini, P.A., Lee, J.H., 2019. Deep neural network predicts emotional responses of the human brain from functional magnetic resonance imaging. NeuroImage 186, 607–627. https://doi.org/10.1016/j.neuroimage.2018.10.054

Kim, J., Calhoun, V.D., Shim, E., Lee, J.H., 2016. Deep neural network with weight sparsity control and pre-training extracts hierarchical features and enhances classification performance: Evidence from whole-brain resting-state functional connectivity patterns of schizophrenia. NeuroImage 124, 127–146. https://doi.org/10.1016/j.neuroimage.2015.05.018

Koo, T.K., Li, M.Y., 2016. A Guideline of Selecting and Reporting Intraclass Correlation Coefficients for Reliability Research. J. Chiropr. Med. 15, 155–163. https://doi.org/10.1016/j.jcm.2016.02.012

Kotov, R., Krueger, R.F., Watson, D., Cicero, D.C., Conway, C.C., Deyoung, C.G., Eaton, N.R., Forbes, M.K., Hallquist, M.N., Latzman, R.D., Mullins-Sweatt, S.N., Ruggero, C.J., Simms, L.J., Waldman, I.D., Waszczuk, M.A., Wright, A.G.C., 2021. The Hierarchical Taxonomy of Psychopathology (HiTOP): A Quantitative Nosology Based on Consensus of Evidence. Annu. Rev. Clin. Psychol. https://doi.org/10.1146/annurev-clinpsy-081219

Kotov, R., Waszczuk, M.A., Krueger, R.F., Forbes, M.K., Watson, D., Clark, L.A., Achenbach, T.M., Althoff, R.R., Ivanova, M.Y., Bagby, R.M., Brown, T.A., Carpenter, W.T., Caspi, A., Moffitt, T.E., Eaton, N.R., Forbush, K.T., Goldberg, D., Hasin, D., Hyman, S.E., Lynam, D.R., Samuel, D.B., South, S.C., Markon, K., Miller, J.D., Morey, L.C., Mullins-Sweatt, S.N., Ormel, J., Patrick, C.J., Regier, D.A., Rescorla, L., Ruggero, C.J., Sellbom, M., Simms, L.J., Skodol, A.E., Slade, T., Tackett, J.L., Waldman, I.D., Widiger, T.A., Wright, A.G.C., Zimmerman, M., 2017. The hierarchical taxonomy of psychopathology (HiTOP): A dimensional alternative to traditional nosologies. J. Abnorm. Psychol. 126, 454–477. https://doi.org/10.1037/abn0000258

Kozak, M.J., Cuthbert, B.N., 2016. The NIMH Research Domain Criteria Initiative: Background, Issues, and Pragmatics. Psychophysiology 53, 286–297. https://doi.org/10.1111/psyp.12518

Kriegeskorte, N., Goebel, R., Bandettini, P., 2006. Information-based functional brain mapping. Proc. Natl. Acad. Sci. 103, 3863–3868. https://doi.org/10.1073/pnas.0600244103

Laceulle, O.M., Chung, J.M., Vollebergh, W.A.M., Ormel, J., 2020. The wide-ranging life outcome correlates of a general psychopathology factor in adolescent psychopathology. Personal. Ment. Health 14, 9–29. https://doi.org/10.1002/pmh.1465

Lees, B., Squeglia, L.M., McTeague, L.M., Forbes, M.K., Krueger, R.F., Sunderland, M., Baillie, A.J., Koch, F., Teesson, M., Mewton, L., 2021. Altered Neurocognitive Functional Connectivity and Activation Patterns Underlie Psychopathology in Preadolescence. Biol. Psychiatry Cogn. Neurosci. Neuroimaging 6, 387–398. https://doi.org/10.1016/j.bpsc.2020.09.007

Marek, S., Tervo-Clemmens, B., Nielsen, A.N., Wheelock, M.D., Miller, R.L., Laumann, T.O., Earl, E., Foran, W.W., Cordova, M., Doyle, O., Perrone, A., Miranda-Dominguez, O., Feczko, E., Sturgeon, D., Graham, A., Hermosillo, R., Snider, K., Galassi, A., Nagel, B.J., Ewing, S.W.F., Eggebrecht, A.T., Garavan, H., Dale, A.M., Greene, D.J., Barch, D.M., Fair, D.A., Luna, B., Dosenbach, N.U.F., 2019. Identifying reproducible individual differences in childhood functional brain networks: An ABCD study. Dev. Cogn. Neurosci. 40. https://doi.org/10.1016/j.dcn.2019.100706

Martino, A.D., Yan, C.G., Li, Q., Denio, E., Castellanos, F.X., Alaerts, K., Anderson, J.S., Assaf, M., Bookheimer, S.Y., Dapretto, M., Deen, B., Delmonte, S., Dinstein, I., Ertl-Wagner, B., Fair, D.A., Gallagher, L., Kennedy, D.P., Keown, C.L., Keysers, C., Lainhart, J.E., Lord, C., Luna, B., Menon, V., Minshew, N.J., Monk, C.S., Mueller, S., Müller, R.A., Nebel, M.B., Nigg, J.T., O'Hearn, K., Pelphrey, K.A., Peltier, S.J., Rudie, J.D., Sunaert, S., Thioux, M., Tyszka, J.M., Uddin, L.Q., Verhoeven, J.S., Wenderoth, N., Wiggins, J.L., Mostofsky, S.H., Milham, M.P., 2014. The autism brain imaging data exchange: Towards a large-scale evaluation of the intrinsic brain architecture in autism. Mol. Psychiatry 19, 659–667. https://doi.org/10.1038/mp.2013.78

Michelini, G., Barch, D.M., Tian, Y., Watson, D., Klein, D.N., Kotov, R., 2019. Delineating and validating higher-order dimensions of psychopathology in the Adolescent Brain Cognitive Development (ABCD) study. Transl. Psychiatry 9. https://doi.org/10.1038/S41398-019-0593-4

Mwansisya, T.E., Hu, A., Li, Y., Chen, X., Wu, G., Huang, X., Lv, D., Li, Z., Liu, C., Xue, Z., Feng, J., Liu, Z., 2017. Task and resting-state fMRI studies in first-episode schizophrenia: A systematic review. Schizophr. Res. 189, 9–18. https://doi.org/10.1016/j.schres.2017.02.026

Norbom, L.B., Doan, N.T., Alnæs, D., Kaufmann, T., Moberget, T., Rokicki, J., Andreassen, O.A., Westlye, L.T., Tamnes, C.K., 2019. Probing Brain Developmental Patterns of Myelination and Associations With Psychopathology in Youths Using Gray/White Matter Contrast. Biol. Psychiatry 85, 389–398. https://doi.org/10.1016/j.biopsych.2018.09.027

Öngür, D., Lundy, M., Greenhouse, I., Shinn, A.K., Menon, V., Cohen, B.M., Renshaw, P.F., 2010. Default mode network abnormalities in bipolar disorder and schizophrenia. Psychiatry Res. Neuroimaging 183, 59–68. https://doi.org/10.1016/j.pscychresns.2010.04.008

Parkes, L., Moore, T.M., Calkins, M.E., Cook, P.A., Cieslak, M., Roalf, D.R., Wolf, D.H., Gur, R.C., Gur, R.E., Satterthwaite, T.D., Bassett, D.S., 2021. Transdiagnostic dimensions of psychopathology explain individuals' unique deviations from normative neurodevelopment in brain structure. Transl. Psychiatry 11. https://doi.org/10.1038/s41398-021-01342-6

Parkes, L., Satterthwaite, T.D., Bassett, D.S., 2020. Towards precise resting-state fMRI biomarkers in psychiatry: synthesizing developments in transdiagnostic research, dimensional models of psychopathology, and normative neurodevelopment. Curr. Opin. Neurobiol. 65, 120–128.

Romer, A.L., Elliott, M.L., Knodt, A.R., Sison, M.L., Ireland, D., Houts, R., Ramrakha, S., Poulton, R., Keenan, R., Melzer, T.R., Moffitt, T.E., Caspi, A., Hariri, A.R., 2021. Pervasively Thinner Neocortex as a Transdiagnostic Feature of General Psychopathology. Am. J. Psychiatry 178, 174–182. https://doi.org/10.1176/appi.ajp.2020.19090934

Satterthwaite, T.D., Connolly, J.J., Ruparel, K., Calkins, M.E., Jackson, C., Elliott, M.A., Roalf, D.R., Hopson, R., Prabhakaran, K., Behr, M., Qiu, H., Mentch, F.D., Chiavacci, R., Sleiman, P.M.A., Gur, R.C., Hakonarson, H., Gur, R.E., 2016. The Philadelphia Neurodevelopmental Cohort: A publicly available resource for the study of normal and abnormal brain development in youth. NeuroImage, Sharing the wealth: Brain Imaging Repositories in 2015 124, 1115–1119. https://doi.org/10.1016/j.neuroimage.2015.03.056

Schulz, M.A., Yeo, B.T.T., Vogelstein, J.T., Mourao-Miranada, J., Kather, J.N., Kording, K., Richards, B., Bzdok, D., 2020. Different scaling of linear models and deep learning in UKBiobank brain images versus machine-learning datasets. Nat. Commun. 11. https://doi.org/10.1038/s41467-020-18037-z

Sha, Z., Wager, T.D., Mechelli, A., He, Y., 2019. Common Dysfunction of Large-Scale Neurocognitive Networks Across Psychiatric Disorders. Biol. Psychiatry 85, 379–388. https://doi.org/10.1016/j.biopsych.2018.11.011

Shaffer, J.J., Johnson, C.P., Fiedorowicz, J.G., Christensen, G.E., Wemmie, J.A., Magnotta, V.A., 2018. Impaired sensory processing measured by functional MRI in Bipolar disorder manic and depressed mood states. Brain Imaging Behav. 12, 837–847. https://doi.org/10.1007/s11682-017-9741-8

Sheline, Y.I., Barch, D.M., Price, J.L., Rundle, M.M., Vaishnavi, S.N., Snyder, A.Z., Mintun, M.A., Wang, S., Coalson, R.S., Raichle, M.E., 2009. The default mode network and self-referential processes in depression. Proc. Natl. Acad. Sci. 106, 1942–1947. https://doi.org/10.1073/pnas.0812686106

Shen, X., Tokoglu, F., Papademetris, X., Constable, R.T., 2013. Groupwise whole-brain parcellation from resting-state fMRI data for network node identification. Neuroimage 82, 403–415.

Smith, D.J., Nicholl, B.I., Cullen, B., Martin, D., Ul-Haq, Z., Evans, J., Gill, J.M.R., Roberts, B., Gallacher, J., Mackay, D., Hotopf, M., Deary, I., Craddock, N., Pell, J.P., 2013. Prevalence and characteristics of probable major depression and bipolar disorder within UK Biobank: Cross-sectional study of 172,751 participants. PLoS ONE 8. https://doi.org/10.1371/journal.pone.0075362

Somerville, L.H., Bookheimer, S.Y., Buckner, R.L., Burgess, G.C., Curtiss, S.W., Dapretto, M., Elam, J.S., Gaffrey, M.S., Harms, M.P., Hodge, C., Kandala, S., Kastman, E.K., Nichols, T.E., Schlaggar, B.L., Smith, S.M., Thomas, K.M., Yacoub, E., Van Essen, D.C., Barch, D.M., 2018. The Lifespan Human Connectome Project in Development: A large-scale study of brain connectivity development in 5–21 year olds. NeuroImage 183, 456–468. https://doi.org/10.1016/j.neuroimage.2018.08.050

Spreng, R.N., Stevens, W.D., Viviano, J.D., Schacter, D.L., 2016. Attenuated anticorrelation between the default and dorsal attention networks with aging: evidence from task and rest. Neurobiol. Aging 45, 149–160. https://doi.org/10.1016/j.neurobiolaging.2016.05.020

Sripada, C., Angstadt, M., Taxali, A., Kessler, D., Greathouse, T., Rutherford, S., Clark, D.A., Hyde, L.W., Weigard, A., Brislin, S.J., Hicks, B., Heitzeg, M., 2021. Widespread attenuating changes in brain connectivity associated with the general factor of psychopathology in 9- and 10-year olds. Transl. Psychiatry 11, 575. https://doi.org/10.1038/s41398-021-01708-w

Thompson, P.M., Jahanshad, N., Ching, C.R.K., Salminen, L.E., Thomopoulos, S.I., Bright, J., Baune, B.T., Bertolín, S., Bralten, J., Bruin, W.B., Bülow, R., Chen, J., Chye, Y., Dannlowski, U., de Kovel, C.G.F., Donohoe, G., Eyler, L.T., Faraone, S.V., Favre, P., Filippi, C.A., Frodl, T., Garijo, D., Gil, Y., Grabe, H.J., Grasby, K.L., Hajek, T., Han, L.K.M., Hatton, S.N., Hilbert, K., Ho, T.C., Holleran, L., Homuth, G., Hosten, N., Houenou, J., Ivanov, I., Jia, T., Kelly, S., Klein, M., Kwon, J.S., Laansma, M.A., Leerssen, J., Lueken, U., Nunes, A., Neill, J.O., Opel, N., Piras, Fabrizio, Piras, Federica, Postema, M.C., Pozzi, E., Shatokhina, N., Soriano-Mas, C., Spalletta, G., Sun, D., Teumer, A., Tilot, A.K., Tozzi, L., van der Merwe, C., Van Someren, E.J.W., van Wingen, G.A., Völzke, H., Walton, E., Wang, L., Winkler, A.M., Wittfeld, K., Wright, M.J., Yun, J.-Y., Zhang, G., Zhang-James, Y., Adhikari, B.M., Agartz, I., Aghajani, M., Aleman, A., Althoff, R.R., Altmann, A., Andreassen, O.A., Baron, D.A., Bartnik-Olson, B.L., Marie Bas-Hoogendam, J., Baskin-Sommers, A.R., Bearden, C.E., Berner, L.A., Boedhoe, P.S.W., Brouwer, R.M., Buitelaar, J.K., Caeyenberghs, K., Cecil, C.A.M., Cohen, R.A., Cole, J.H., Conrod, P.J., De Brito, S.A., de Zwarte, S.M.C., Dennis, E.L., Desrivieres, S., Dima, D., Ehrlich, S., Esopenko, C., Fairchild, G., Fisher, S.E., Fouche, J.-P., Francks, C., Frangou, S., Franke, B., Garavan, H.P., Glahn, D.C., Groenewold, N.A., Gurholt, T.P., Gutman, B.A., Hahn, T., Harding, I.H., Hernaus, D., Hibar, D.P., Hillary, F.G., Hoogman, M., Hulshoff Pol, H.E., Jalbrzikowski, M., Karkashadze, G.A., Klapwijk, E.T., Knickmeyer, R.C., Kochunov, P., Koerte, I.K., Kong, X.-Z., Liew, S.-L., Lin, A.P., Logue, M.W., Luders, E., Macciardi, F., Mackey, S., Mayer, A.R., McDonald, C.R., McMahon, A.B., Medland, S.E., Modinos, G., Morey, R.A., Mueller, S.C., Mukherjee, P., Namazova-Baranova, L., Nir, T.M., Olsen, A., Paschou, P., Pine, D.S., Pizzagalli, F., Rentería, M.E., Rohrer, J.D., Sämann, P.G., Schmaal, L., Schumann, G., Shiroishi, M.S., Sisodiya, S.M., Smit, D.J.A., Sønderby, I.E., Stein, D.J., Stein, J.L., Tahmasian, M., Tate, D.F., Turner, J.A., van den Heuvel, O.A., van der Wee, N.J.A., van der Werf, Y.D., van Erp, T.G.M., van Haren, N.E.M., van Rooij, D., van Velzen, L.S., Veer, I.M., Veltman, D.J., Villalon-Reina, J.E., Walter, H., Whelan, C.D., Wilde, E.A., Zarei, M., Zelman, V., 2020. ENIGMA and global neuroscience: A decade of large-scale studies of the brain in health and disease across more than 40 countries. Transl. Psychiatry 10, 1–28. https://doi.org/10.1038/s41398-020-0705-1

Tzourio-Mazoyer, N., Landeau, B., Papathanassiou, D., Crivello, F., Etard, O., Delcroix, N., Mazoyer, B., Joliot, M., 2002. Automated anatomical labeling of activations in SPM using a macroscopic anatomical parcellation of the MNI MRI single-subject brain. Neuroimage 15, 273–289.

Uddin, L.Q., Kelly, A.M.C., Biswal, B.B., Margulies, D.S., Shehzad, Z., Shaw, D., Ghaffari, M., Rotrosen, J., Adler, L.A., Castellanos, F.X., Milham, M.P., 2008. Network homogeneity reveals decreased integrity of default-mode network in ADHD. J. Neurosci. Methods 169, 249–254. https://doi.org/10.1016/j.jneumeth.2007.11.031

van de Ven, V., Rotarska Jagiela, A., Oertel-Knöchel, V., Linden, D.E.J., 2017. Reduced intrinsic visual cortical connectivity is associated with impaired perceptual closure in schizophrenia. NeuroImage Clin. 15, 45–52. https://doi.org/10.1016/j.nicl.2017.04.012

Vu, H., Kim, H.-C., Jung, M., Lee, J.-H., 2020. fMRI volume classification using a 3D convolutional neural network robust to shifted and scaled neuronal activations. NeuroImage 223, 117328. https://doi.org/10.1016/j.neuroimage.2020.117328

Wang, L., Lin, F.V., Cole, M., Zhang, Z., 2021. Learning Clique Subgraphs in Structural Brain Network Classification with Application to Crystallized Cognition. NeuroImage 225, 117493. https://doi.org/10.1016/j.neuroimage.2020.117493

Whitfield-Gabrieli, S., Ford, J.M., 2012. Default Mode Network Activity and Connectivity in Psychopathology. Annu. Rev. Clin. Psychol. 8, 49–76. https://doi.org/10.1146/annurev-clinpsy-032511-143049

Xia, C.H., Ma, Z., Ciric, R., Gu, S., Betzel, R.F., Kaczkurkin, A.N., Calkins, M.E., Cook, P.A., Garza, A.G. de la, Vandekar, S.N., Cui, Z., Moore, T.M., Roalf, D.R., Ruparel, K., Wolf, D.H., Davatzikos, C., Gur, R.C., Gur, R.E., Shinohara, R.T., Bassett, D.S., Satterthwaite, T.D., 2018. Linked dimensions of psychopathology and connectivity in functional brain networks. Nat. Commun. 9. https://doi.org/10.1038/s41467-018-05317-y

Yu, M., Linn, K.A., Cook, P.A., Phillips, M.L., McInnis, M., Fava, M., Trivedi, M.H., Weissman, M.M., Shinohara, R.T., Sheline, Y.I., 2018. Statistical harmonization corrects site effects in functional connectivity measurements from multi-site fMRI data. Hum. Brain Mapp. 39, 4213–4227. https://doi.org/10.1002/hbm.24241

Zelazo, P.D., 2020. Executive Function and Psychopathology: A Neurodevelopmental Perspective. Annu. Rev. Clin. Psychol. 16, 431–454. https://doi.org/10.1146/annurev-clinpsy-072319-024242

Zhao, K., Duka, B., Xie, H., Oathes, D.J., Calhoun, V., Zhang, Y., 2022. A dynamic graph convolutional neural network framework reveals new insights into connectome dysfunctions in ADHD. NeuroImage 246, 118774. https://doi.org/10.1016/j.neuroimage.2021.118774

Zhao, Q., Adeli, E., Pohl, K.M., 2020. Training confounder-free deep learning models for medical applications. Nat. Commun. 11. https://doi.org/10.1038/s41467-020-19784-9

# Figure legends

**Figure 1**. The number of participants by site and the SGNN architecture. (A) The number of subjects for each of the 18 included sites scanned with either the Siemens or GE scanner. (B) The number of male and female subjects acquired using each of the two scanners. (C) RSFC data were extracted from the preprocessed rfMRI data using the 352 ROIs. (D) Schematic of the SGNN. The vectorized RSFC (dim = 61,776) was used as input for the SGNN. In the training phase of the SGNN, the feature extractor layer learned the features of the RSFC input to predict the *p*-factor and remove scanner-induced heterogeneity via the subsequent *p*-factor predictor and scanner discriminator branches, respectively. The *p*-factor predictor has only one output node with a linear activation function to predict the *p*-factor. The scanner discriminator has two output nodes with a softmax layer for the binary classification of the scanner labels. SGNN, scanner-generalization neural network; RSFC, resting-state functional connectivity; rfMRI, resting-state functional magnetic resonance imaging; ROIs, regions-of-interest; *p*-factor, general psychopathology factor.

**Figure 2**. The LOSOCV and LTSOCV frameworks and weight feature (WF) representation for the SGNN. (A) Two nested CV schemes were used to train, validate, and test the SGNN and machine learning models. The hyperparameters of the models were optimized in the inner CV loop based on the validation performance, and the optimized model was tested in the outer CV loop using the test data. (B) The WF representation was calculated for the *p*-factor predictor and scanner discriminator branches of the SGNN by multiplying the weight matrices in each branch. LOSOCV, leave-one-site-out cross-validation; LTSOCV, leave-two-site-out cross-validation; SGNN, scanner-generalization neural network; PP, *p*-factor predictor; SCD, scanner discriminator.

**Figure 3**. The *p*-factor prediction performance of the models with LOSOCV. (A) The CCs for the target and predicted *p*-factors are presented as a box-whisker plot (left; inter-quartile range as the box with the median and $10^{th}$ and $90^{th}$ percentiles as the whiskers) and a bar plot (right; average CC). The SGNN model achieved a significantly higher average test CC (CC = 0.1631 ± 0.0673) than the best performing KRR model (CC = 0.1497 ± 0.0710; $p < 0.05$; two-tailed paired sample *t*-test). (B) Bar graphs for the MAE for the target and predicted *p*-factors. The SGNN model exhibited a significantly lower MAE (MAE = 0.7411 ± 0.0433) than the best performing KRR model (MAE = 0.7432 ± 0.0438; $p < 0.05$). CCs, Pearson's correlation coefficients; MAE, mean absolute error; KRR, kernel ridge regression; LR, linear regression; $LR_{Ridge}$, LR with L2-norm regularization; $LR_{Lasso}$, LR with L1-norm regularization; SVR, support vector machine-based regression; $PLS_{Reg}$, partial least square-based regression; SGNN, scanner-generalization neural network.

**Figure 4**. Hyperparameter tuning and pre-training of the SGNN with LOSOCV. The CCs (A) for the training and (B) validation phases depending on the weight sparsity level for the FE are shown. (C) The number of selected folds for the optimal lambda (λ) value. (D) CCs for the training and validation phases for each of the λ values (mean ± standard error). (E) Scanner discrimination performance based on the λ value. (F) CC performance curves for each of the two pre-training schemes. CCs, Pearson's correlation coefficients; HSP, Hoyer's sparseness level of the weight; FE, feature extractor; PRT, pre-training; PP, *p*-factor predictor; SCD, scanner discriminator.

**Figure 5**. The representative weight features (WFs) for the *p*-factor predictor (PP) in the SGNN with LOSOCV. The WFs are presented (A) at the functional network (FN) level and (B,C) at a region-of-interest (ROI) level as a circular graph and on the cortical surface, respectively. Please refer to the subsections "***2.6. Interpretation of the trained SGNN***" and "***3.3. Important FNs for p-factor prediction and scanner generalization***" for more detail. LOSOCV, leave-one-site-out cross-validation.

**Figure 6**. The representative weight features (WFs) for the scanner discriminator in the SGNN with LOSOCV. The WFs are presented (A) at the functional network (FN) level and (B,C) at a region-of-interest (ROI) level as a circular graph and on the cortical surface, respectively. Please refer to the subsections "***2.6. Interpretation of the trained SGNN***" and "***3.3. Important FNs for p-factor prediction and scanner generalization***" for more detail. LOSOCV, leave-one-site-out cross-validation.

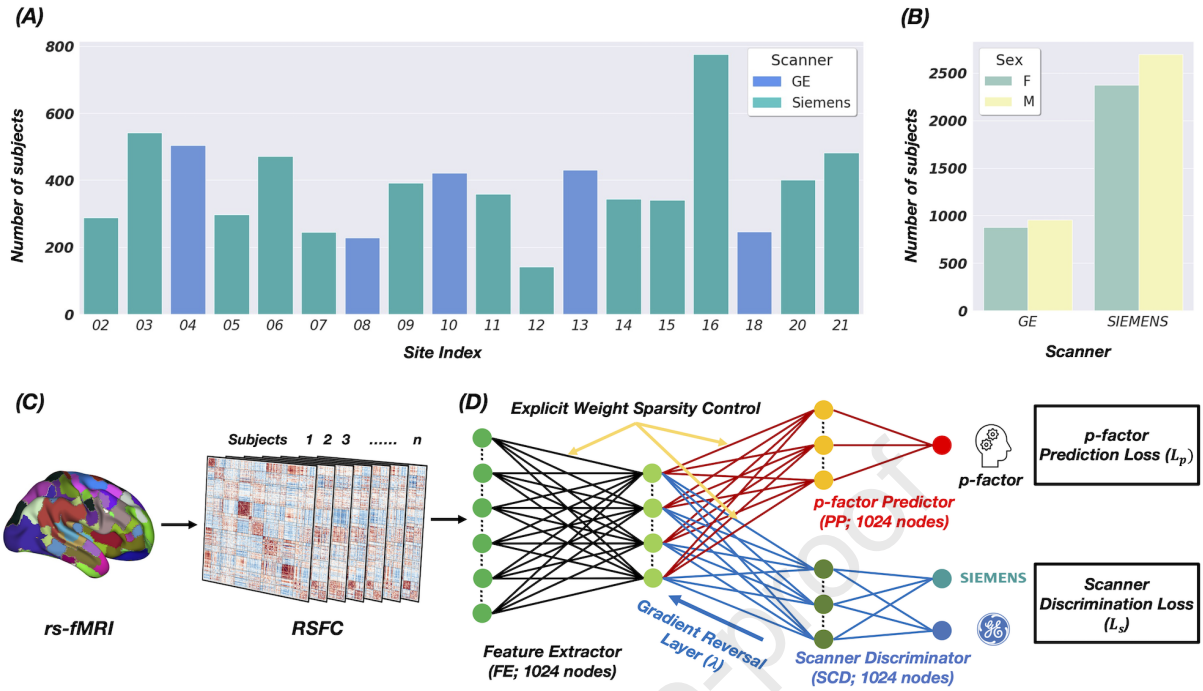

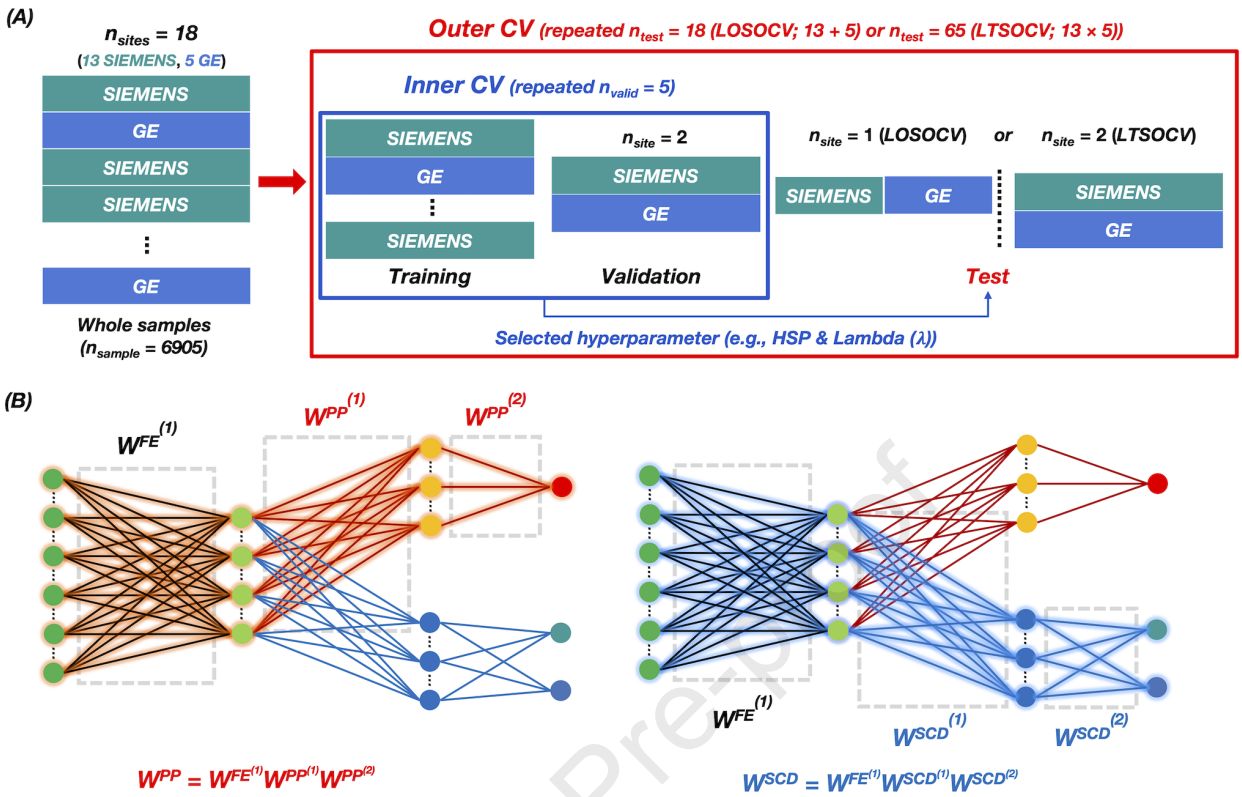

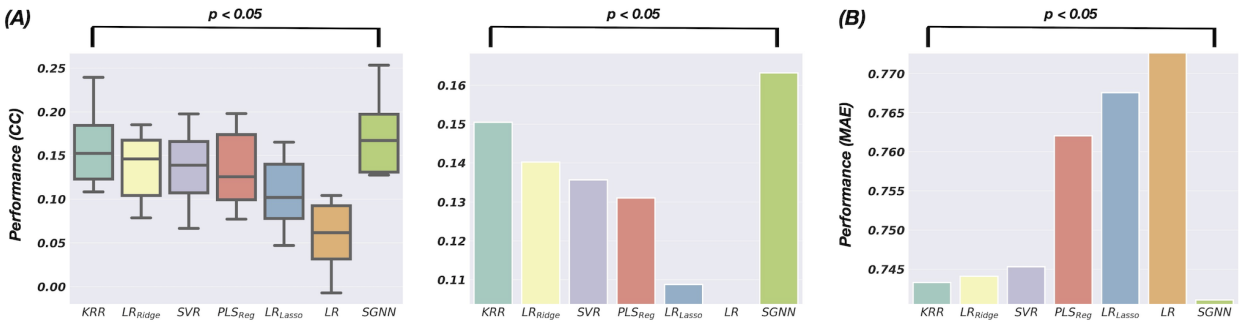

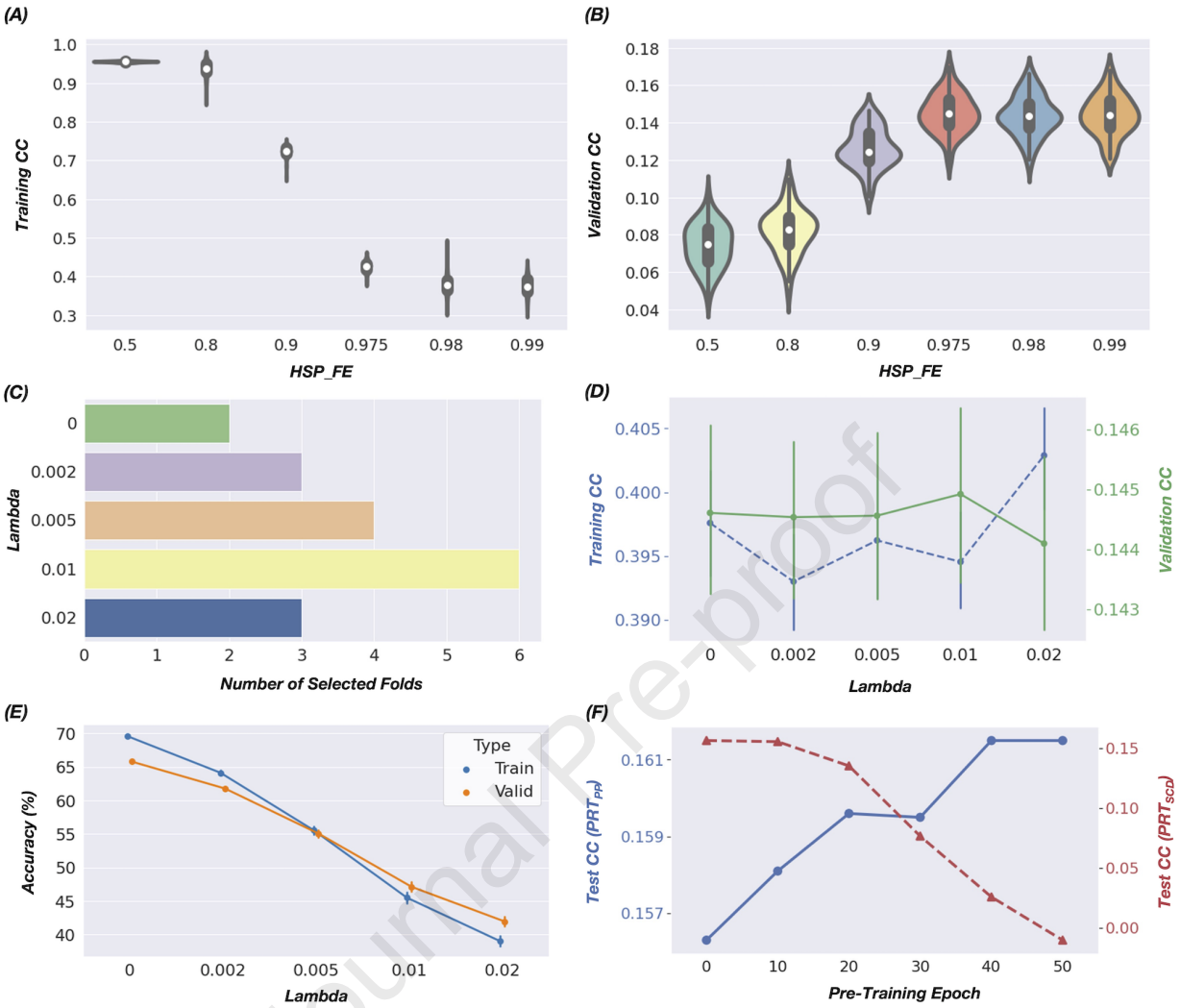

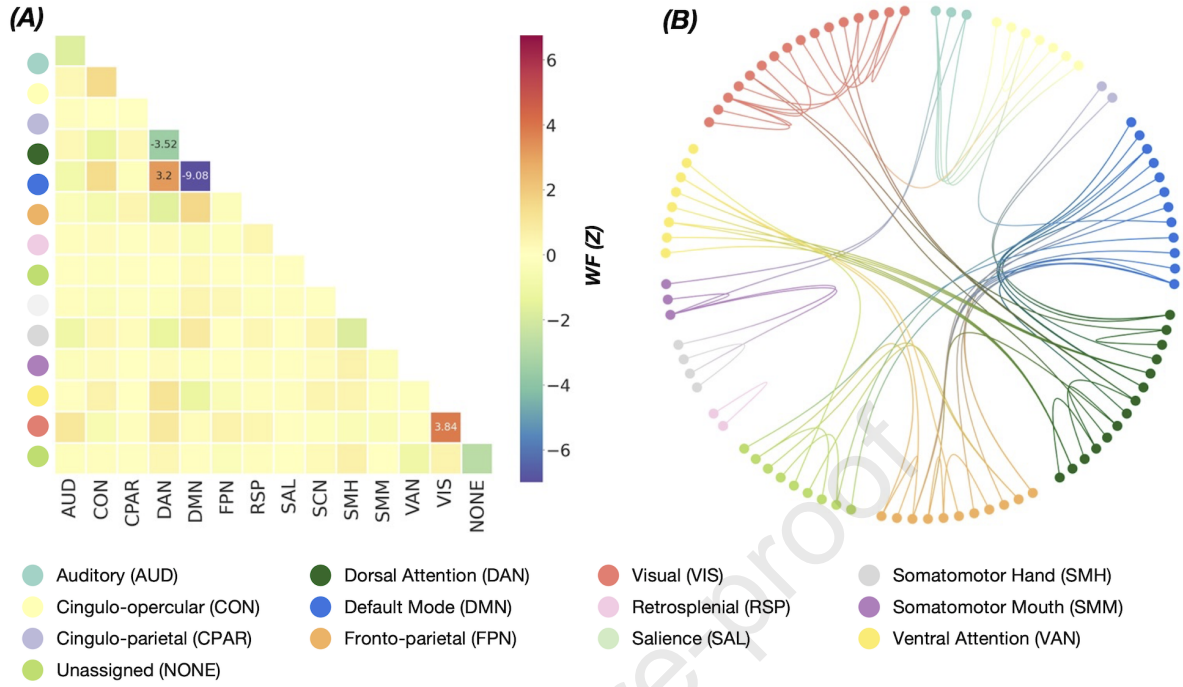


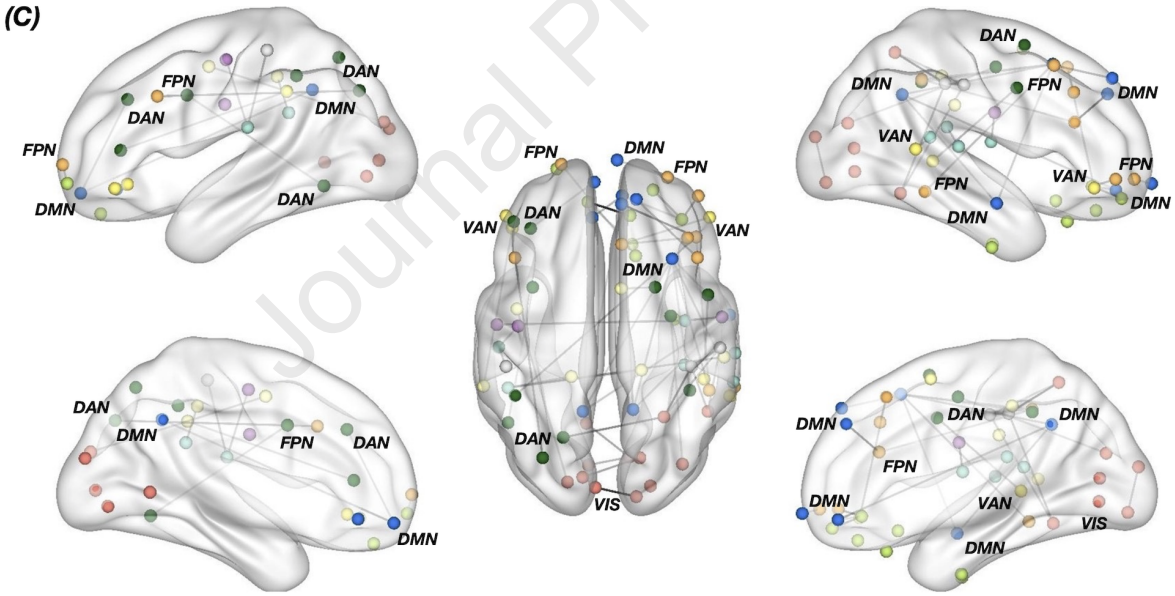

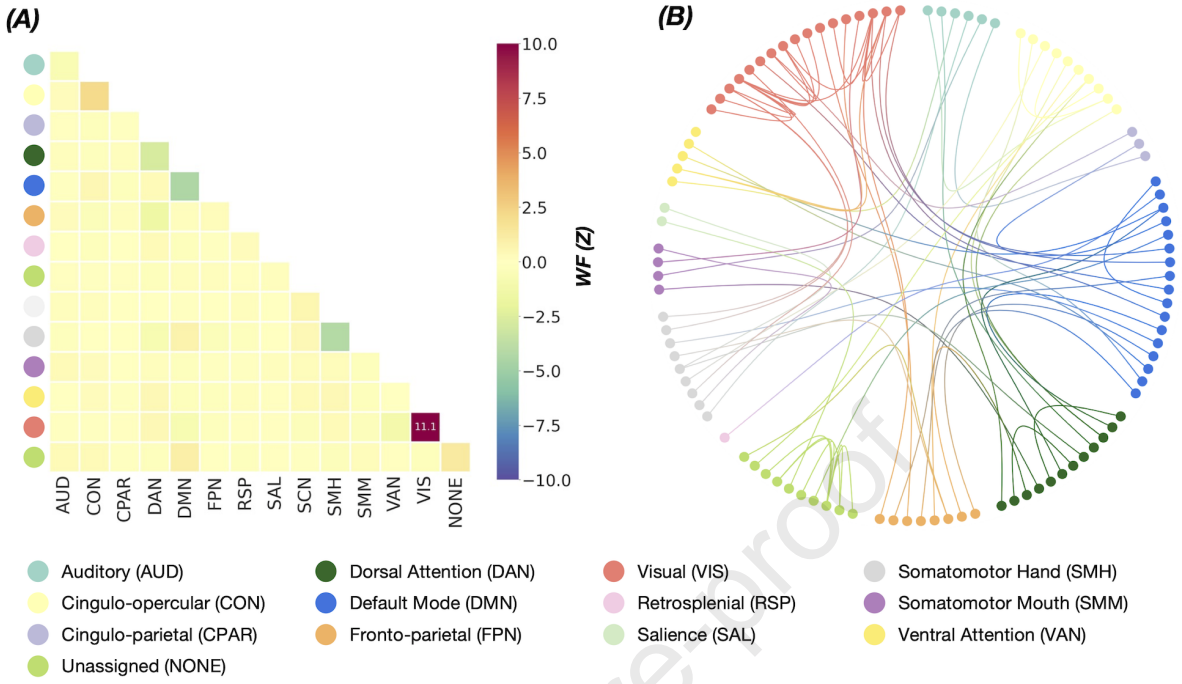


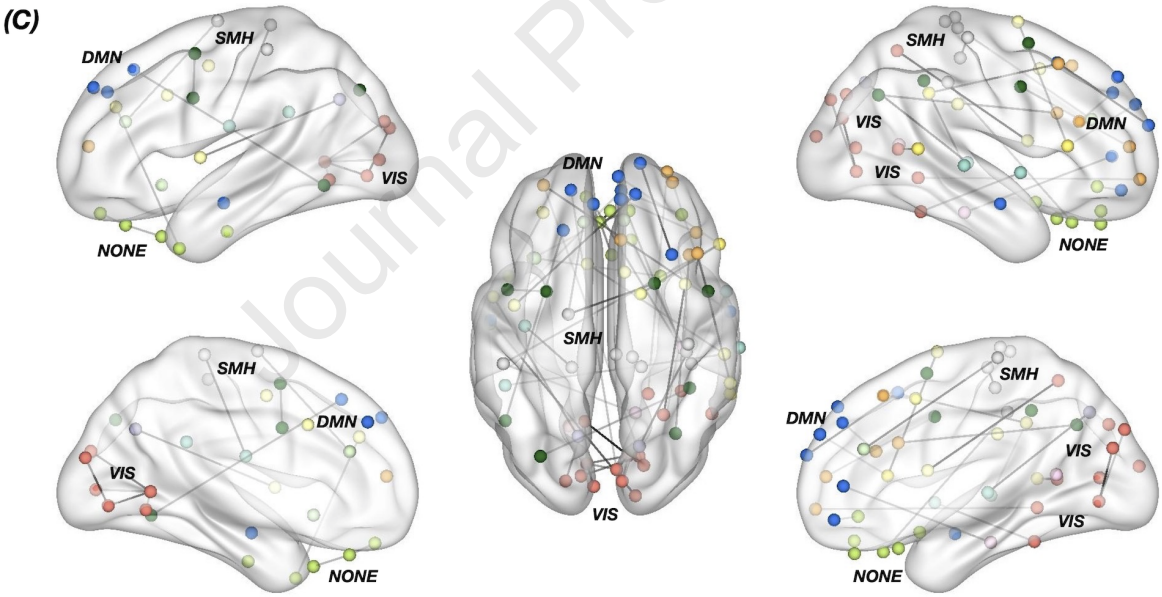

**Jinwoo Hong**: Conceptualization, Data curation, Formal analysis, Investigation, Methodology, Software, Validation, Visualization, Writing-Original Draft, Writing-Review & Editing,

**Jundong Hwang**: Data curation, Writing - review & editing

**Jong-Hwan Lee**: Conceptualization, Funding acquisition, Investigation, Resources, Supervision, Writing - original draft, Writing - review & editing

**Declaration of interests**

☒ The authors declare that they have no known competing financial interests or personal relationships that could have appeared to influence the work reported in this paper.

☐ The authors declare the following financial interests/personal relationships which may be considered as potential competing interests: